Synthesis, Molecular and Electronic Structure of U-V(O)[N(SiMe3)(2)](3)

ARTICLE *in* INORGANIC CHEMISTRY · FEBRUARY 2012

Impact Factor: 4.76 · DOI: 10.1021/ic201936j · Source: PubMed

5 AUTHORS, INCLUDING:

Jessie L. McDonald (Brown)
Transylvania University
13 PUBLICATIONS **213** CITATIONS

SEE PROFILE

Inorganic Chemistry

Article

pubs.acs.org/IC

Synthesis, Molecular and Electronic Structure of $U^{V}(O)[N(SiMe_3)_2]_3$

Skye Fortier,[†] Jessie L. Brown,[†] Nikolas Kaltsoyannis,*[,‡] Guang Wu,[†] and Trevor W. Hayton*[,†]

[†]Department of Chemistry and Biochemistry, University of California, Santa Barbara, California 93106, United States

[‡]Department of Chemistry, Christopher Ingold Laboratories, University College London, 20 Gordon Street, London WC1H 0AJ, United Kingdom

Supporting Information

ABSTRACT: Addition of 1 equiv of 2,2,6,6-tetramethylpiperidine-1-oxyl (TEMPO) to $U(NR_2)_3$ in hexanes affords $U(O)(NR_2)_3$ (**2**), which can be isolated in 73% yield. Complex **2** is a rare example of a terminal U(V) oxo complex. In contrast, addition of 1 equiv of Me_3NO to $U(NR_2)_3$ (R = $SiMe_3$) in pentane generates the U(IV) bridging oxo $[(NR_2)_3U]_2(\mu\text{-}O)$ (**3**) in moderate yields. Also formed in this reaction, in low yield, is the U(IV) iodide complex $U(I)(NR_2)_3$ (**4**). The iodide ligand in **4** likely originates from residual NaI, present in the $U(NR_2)_3$ starting material. Complex **4** can be generated rationally by addition of 0.5 equiv of I_2 to a hexane solution of $U(NR_2)_3$, where it can be isolated in moderate yield as a tan crystalline solid. The solid-state molecular structures and magnetic susceptibilities of **2**, **3**, and **4** have been measured. In addition, the electronic structures of **2** and **3** have been investigated by density functional theory (DFT) methods.

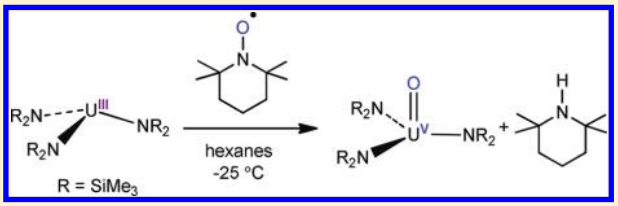

INTRODUCTION

While the trans-di(oxo) framework of the uranyl ion is ubiquitous in uranium chemistry,[1−3] terminal mono-oxo complexes of uranium are surprisingly rare.[4] This is probably due, in part, to the potent nucleophilicity of the oxo ligands in these species,[5−7] which necessitates the use of bulky ancillary ligands to prevent the formation of bridging oxo groups.[5,6,8−13] For example, $Cp'_2U(bipy)$, where Cp′ is the extremely bulky 1,2,4-$^{t}Bu_3C_5H_2$ cyclopentadienyl ligand, reacts with pyridine-*N*-oxide in Et_2O to provide the terminal oxo $Cp'_2U(O)(py)$ in good yield.[5,14] Interestingly, the oxo ligand in the base-free analogue, $Cp'_2U(O)$, rapidly reacts with Me_3SiCl to give $Cp'_2U(OSiMe_3)(Cl)$, confirming the nucleophilicity of this functional group.[5,14] The identity of the O-atom source is also important in determining whether a terminal oxo ligand is formed upon atom transfer. For example, the synthesis of a terminal oxo can be achieved by addition of CO_2 to a U(V) imido, $((^{tBu}ArO)_3tacn)U(NMes)$.[15] This results in the formation of mesityl isocyanate and a U(V) terminal oxo complex via a [2 + 2] cycloaddition. In contrast, addition of an O-atom transfer reagent to the U^{III} parent complex generates a U(IV) bridging oxo species, $[((^{tBu}ArO)_3tacn)U]_2(\mu\text{-}O)$, and not the U(V) terminal oxo.[16,17] Addition of N_2O to $((^{tBu}ArO)_3mes)U$ also results in the formation of a U(IV) bridging oxo, $[((^{tBu}ArO)_3mes)U]_2(\mu\text{-}O)$.[7] Similarly, addition of H_2O to $[U(tpa)_2]I_3$, (tpa = tris[(2-pyridyl)methyl]amine), results in the formation of a U(IV) bridged oxo cluster.[18,19]

Recently, we described the synthesis of a terminal U(V) oxo complex $[Ph_3PCH_3][U(O)(CH_2SiMe_2NSiMe_3)(N\{SiMe_3\}_2)_2]$ (**1**) (Chart 1)[20] by O-atom transfer from TEMPO (TEMPO = 2,2,6,6-tetramethylpiperidine-1-oxyl). While the O-atom transfer ability of TEMPO has only been documented in a few instances,[21,22] this preliminary result suggests that the reaction of TEMPO with other actinide complexes may be a fruitful arena for the generation of new terminal oxos. Previously, Evans and co-workers demonstrated that reaction of TEMPO with Cp^*_3Sm results in ligand oxidation and formation of $[Sm(TEMPO)_3]_2$.[23] However, no evidence for N−O bond cleavage was observed in this example.

Chart 1

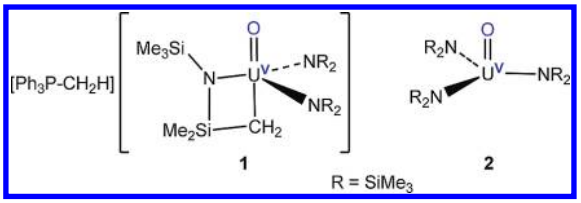

The isolation of complex **1**,[20] prompted us to investigate the chemistry of the closely related U(V) oxo $U(O)(NR_2)_3$ (R = $SiMe_3$) (**2**). Despite being reported by Andersen in 1979,[24] this complex has received little attention, and both its chemistry and solid-state structure have yet to be elaborated. This is surprising given the paucity of uranium complexes with mono-oxo functionalities and the current interest in molecular U(V) systems.[4,25−31] Herein, we revisit the synthesis of $U(O)(NR_2)_3$ (R = $SiMe_3$) (**2**) and explore its electronic structure with Density Functional Theory (DFT).

RESULTS AND DISCUSSION

Following the literature procedure for the synthesis of **2**,[24] 1 equiv of Me_3NO was added to $U(NR_2)_3$ (R = $SiMe_3$) in pentane, generating a dark brown-red solution. Consistent with the previous report, light yellow crystals were isolated from the reaction mixture. Surprisingly, however, an X-ray crystallographic

Received: September 2, 2011
Published: January 13, 2012

   dx.doi.org/10.1021/ic201936j | *Inorg. Chem.* 2012, 51, 1625−1633

analysis of the material indicated that a U(IV) bridging oxide $[(NR_2)_3U]_2(\mu\text{-}O)$ (**3**) was generated, instead of the anticipated U(V) terminal oxo complex. Complex **3** can also be synthesized, in slightly better yield, via the treatment of $U(NR_2)_3$ with 0.5 equiv of Me_3NO (Scheme 1). Interestingly, the oxidation of

Scheme 1

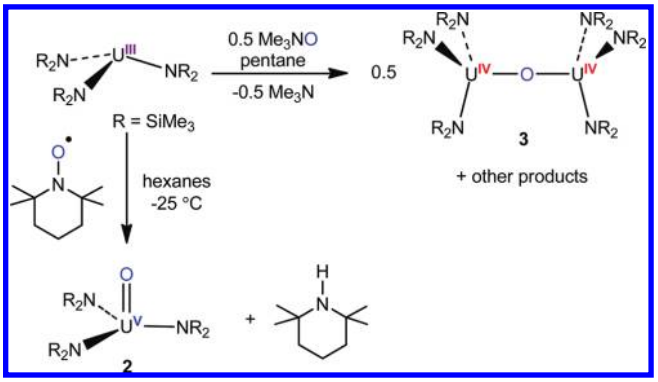

the related U(III) tris(amide), $U(NN'_3)$ ($NN'_3 = N(CH_2CH_2NR)_3$, $R = SiMe_2{}^tBu$), with 1 equiv of Me_3NO also yields a U(IV) bridging oxo complex, $[(NN'_3)U]_2(\mu\text{-}O)$.[32]

Complex **3** crystallizes in the monoclinic space group *C*2/*c* with two independent molecules in the asymmetric unit. The solid-state molecular structure of **3** reveals that each U(IV) center possesses a pseudotetrahedral geometry comprised of a bridging O^{2-} group and three silylamide ligands (Figure 1). Additionally,

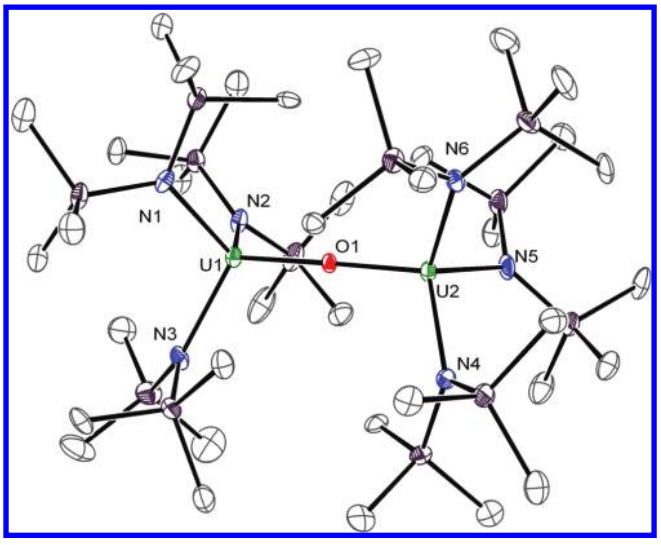

Figure 1. ORTEP diagram of $[(NR_2)_3U]_2(\mu\text{-}O)\cdot 2.5C_6D_6$ ($R = SiMe_3$) (**3**·2.5C_6D_6) represented with 50% probability ellipsoids. Hydrogen atoms and solvent molecules omitted for clarity. Selected bond lengths (Å) and angles (deg): U1−O1 = 2.142(6), U2−O1 = 2.147(6), U1−N1 = 2.295(8), U1−N2 = 2.27(1), U1−N3 = 2.297(8), U2−N4 = 2.273(8), U2−N5 = 2.290(8), U2−N6 = 2.293(8), O1−U1−N1 = 115.1(3), O1−U1−N2 = 112.2(3), O1−U1−N3 = 112.1(3), O1−U2−N4 = 113.5(3), O1−U2−N5 = 112.8(3), O1−U2−N6 = 113.8(3), U1−O1−U2 = 179.2(4).

the complex exhibits a linear U−O−U bond angle (e.g., U1−O1−U2 = 179.2(4)°) with U−O distances (e.g., U1−O1 = 2.142(6) Å, U1−O2 = 2.147(6) Å) similar to that found for the related U(IV) bridging oxo $[((^{tBu}ArO)_3tacn)U]_2(\mu\text{-}O)$ (U−O = 2.1095(4) Å).[33]

The room temperature ^1H NMR spectrum of **3** in C_7D_8 displays four broad resonances at −28.64, −16.79, −6.50, and 15.23 ppm, occurring in a 1:1:1:3 ratio, respectively. These relative ratios can be explained by assuming that rotation along the U−N bonds is restricted, affording two sets of $SiMe_3$ groups in a 3:3 ratio: one group that points toward (*endo*) the oxo bridge and one group that points away (*exo*) from the oxo bridge. Additionally, slow rotation about the $N-Si_{endo}$ bonds, because of the interdigitation of the methyl substituents, further splits the *endo* $SiMe_3$ group into three inequivalent methyl environments, thereby accounting for the overall 1:1:1:3 ratio. Consistent with this analysis, heating the solution to 45 °C results in the coalescence of the peaks at −28.64, −16.79, −6.50 ppm into a very broad resonance at −14.05 ppm, as expected upon faster rotation of $N-Si_{endo}$ bonds. Moreover, cooling the solution to −55 °C produces six well-resolved resonances of equal intensity, ranging from −43.23 to 80.61 ppm, assignable to the three *endo* and three *exo* methyl environments and consistent with slow rotation of both the $N-Si_{endo}$ and $N-Si_{exo}$ bonds.

The effective magnetic moment (μ_{eff}) for **3** is 1.92 μ_B per U^{4+} ion at 300 K (Figure 2), as determined by SQUID magneto-

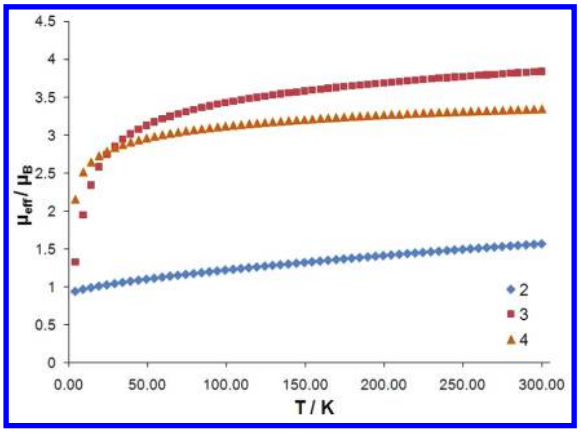

Figure 2. Temperature-dependent SQUID magnetization data for U(O)-$(NR_2)_3$ ($R = SiMe_3$) (**2**), $[(NR_2)_3U]_2(\mu\text{-}O)$ (**3**), and $U(I)(NR_2)_3$ (**4**).

metry, which is comparable to the 1.82 μ_B reported for Andersen's oxo complex.[24] Both values are well below the 3.54 μ_B expected for a free U^{4+} ion,[34,35] but are within the lower range established for U(IV) complexes (e.g., μ_{eff} = 1.98 μ_B for $[Li(THF)]_2[U(O^tBu)_6]$).[36] Additionally, the IR spectrum of **3** (KBr pellet) exhibits an absorption at 932 cm^{-1}, matching a band originally assigned to the terminal U═O stretch of **2** at 930 cm^{-1}. However, the parent U(III) tris(amide), $U(NR_2)_3$, also exhibits a band at 930 cm^{-1} (see the Supporting Information) suggesting this stretch is assignable to the absorptions of the silylamide ligand, rather than a U−O stretch. Finally, the melting point for **3** was determined to be 155−157 °C, nearly identical to that reported by Andersen for the putative terminal oxo (157−159 °C). Overall, the similarity of our characterization data with that reported by Andersen, and the similar appearance of **3** with Andersen's material (green-yellow prisms), suggests that the material originally reported in 1979 may have been complex **3**, and not the terminal U(V) oxo species **2** as originally proposed.

To gain further insight into the electronic and geometric structure of **3** we have performed gradient-corrected DFT calculations. Geometry optimization of a quintet state in the D_3 point group yielded excellent agreement with experiment (U−O = 2.164 Å calc, 2.145 Å exp (av.); U−N = 2.301 Å calc,

dx.doi.org/10.1021/ic201936j | Inorg. Chem. 2012, 51, 1625−1633

2.286 Å exp (av.); O−U−N = 113.0° calc, 113.3° exp (av.)), and subsequent calculation of the vibrational frequencies revealed no imaginary modes. The four unpaired electrons are almost entirely metal-localized (>90% in all cases), with a uranium Mulliken spin density of 2.21 per metal center. There are no calculated vibrational frequencies between 880 cm^{-1} and 1214 cm^{-1}; vibrations at 853 cm^{-1} and 855 cm^{-1}, predicted to yield very intense infrared bands, are associated with modes contained within the silylamide ligands, and are most likely the cause of the band observed experimentally at 932 cm^{-1}.

To better understand the formation of **3**, the reaction of $U(NR_2)_3$ with 0.5 equiv of Me_3NO was followed by ^1H NMR spectroscopy in C_6D_6. Under these conditions several products are formed during the reaction, and in addition to the resonances of **3**, resonances assignable to the U(IV) metallacycle $U(CH_2SiMe_2NR)(NR_2)_2$ are also observed.[37,38] No evidence for the presence of **2** (vide infra), even in small amounts, is observed in these spectra. This is true, regardless of whether 0.5 equiv or 1 equiv of Me_3NO is used in the reaction. Interestingly, we have found that these samples often exhibit a sharp singlet at −0.98 ppm in their ^1H NMR spectra. Moreover, the intensity of this resonance is highly dependent on the batch of $U(NR_2)_3$ used in the synthesis of **3**. We have identified this resonance as corresponding to the U(IV) iodide complex $U(I)(NR_2)_3$ (**4**). The iodide ligand in **4** likely originates from NaI, which is present in the $U(NR_2)_3$ starting material and can be difficult to completely remove by recrystallization. In support of this hypothesis, treatment of $U(NR_2)_3$ with 1 equiv of NaI, followed by 0.5 equiv of Me_3NO, generates **4** (Scheme 2) as the major product, as indicated by

Scheme 2

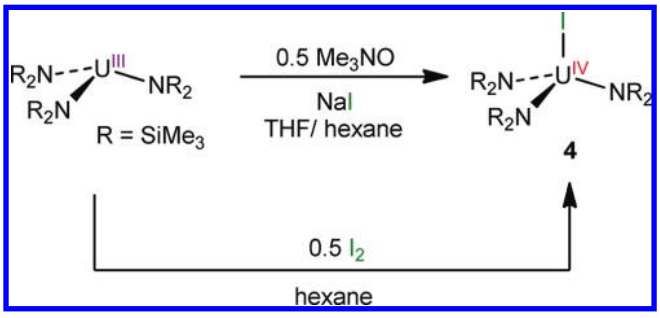

analysis of the crude reaction mixture by ^1H NMR spectroscopy (see the Supporting Information). However, the formation of **3** is not completely suppressed under these conditions. More importantly, complex **3** is also still formed if sublimed $U(NR_2)_3$ is used in place of material that was only recrystallized from hexane, demonstrating that the presence of NaI is not required for the formation of **3** (see the Supporting Information). Interestingly, under these conditions very small amounts of **2** are observed in the supernatant by ^1H NMR spectroscopy.

Complex **4** can be rationally synthesized by addition of 0.5 equiv of I_2 to a hexane solution of $U(NR_2)_3$ (Scheme 2). Recrystallization from CH_2Cl_2 affords **4** as light tan crystals in 62% yield. Its room temperature ^1H NMR spectrum in C_6D_6 exhibits a singlet at −0.98 ppm, identical to that observed in the crude samples of **3**. Analysis by X-ray crystallography (Figure 3) reveals that complex **4** adopts a pseudotetrahedral geometry in the solid-state (I1−U1−N1 = 101.8(1)°, N1−U1−N1* = 115.96(8)°), similar to other four-coordinate silylamide complexes.[39] Additionally, **4** exhibits an effective magnetic moment of 3.35 μ_B at 300 K, which

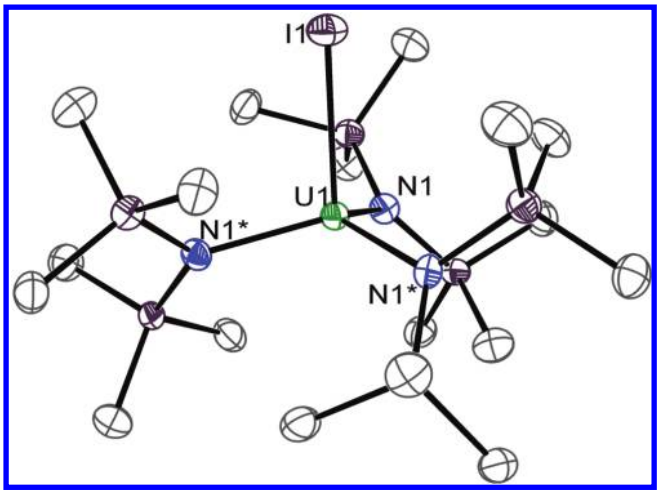

Figure 3. ORTEP diagram of $U(I)(NR_2)_3$ (R = $SiMe_3$) (**4**) with 50% probability ellipsoids. Hydrogen atoms omitted for clarity. Selected bond lengths (Å) and angles (deg): U1−I1 = 2.9512(8), U1−N1 = 2.238(4), I1−U1−N1 = 101.8(1), N1−U1−N1* = 115.96(8).

decreases to 2.16 μ_B at 4 K (Figure 2); fully consistent with the U(IV) oxidation state assignment.[7,35,40−42]

The failure to generate **2** from $U(NR_2)_3$ and Me_3NO compelled us to investigate the use of other O-atom transfer reagents. As demonstrated by the synthesis of **1**,[20] TEMPO can be an effective O-atom source for the actinides. Thus, addition of 1 equiv of TEMPO to $U(NR_2)_3$ in hexane initially affords a pale orange solution. Within seconds, however, this orange solution converts to a dark red color. Crystallization from hexane at −25 °C results in the deposition of **2** as red blocks in 73% yield (Scheme 1). Notably, the appearance of **2** is substantially different than that originally reported for this material.[24] Complex **2** is also formed if sublimed $U(NR_2)_3$ is used in place of recrystallized $U(NR_2)_3$. The ^1H NMR spectrum of **2** in C_6D_6 exhibits a single resonance at −0.23 ppm. Interestingly, in solution at room temperature, **2** slowly decomposes over 24 h, affording HNR_2 and the U(IV) metallacycle $U(CH_2SiMe_2NR)(NR_2)_2$ as the major products (see Supporting Information, Figure S2). Preliminary reactivity studies show that **2** readily conproportionates with $U(NR_2)_3$ to produce **3** (Scheme 3). Furthermore, treatment of **2** with 1 equiv of $Ph_3P{=}CH_2$ in C_6D_6 rapidly generates **1** via deprotonation of a silylamide ligand (Scheme 3). Finally, the melting point for **2** was determined to be 104−105 °C.

The synthesis of **2** is also accompanied with the formation of tetramethylpiperidine (TMPH), as revealed by ^1H NMR spectroscopy. Its presence can be explained by invoking formation of the TMP· radical upon O-atom transfer, followed by abstraction of H· from the solvent.[21] Not surprisingly, performing the reaction in the presence of 9,10-dihydroanthracene affords the coupled product 9,9′,10,10′-tetrahydro-9,9′-bianthracene, formed as a result of H· abstraction by TMP· (see Supporting Information, Figure S3).[20,43]

To account for the formation of complexes **2** and **3** we suggest that the relative rates of uranium binding and N−O bond cleavage between TEMPO and Me_3NO are responsible for the different reaction outcomes. Accordingly, during the reaction of TEMPO with $U(NR_2)_3$, TEMPO coordination is rapid, quickly consuming all the $U(NR_2)_3$ in solution. However, subsequent N−O bond cleavage occurs at a slower rate, selectively generating $U(NR_2)_3(O)$ as the only uranium-containing product. This hypothesis is supported by the observation of a pale orange

dx.doi.org/10.1021/ic201936j | Inorg. Chem. 2012, 51, 1625−1633

Scheme 3

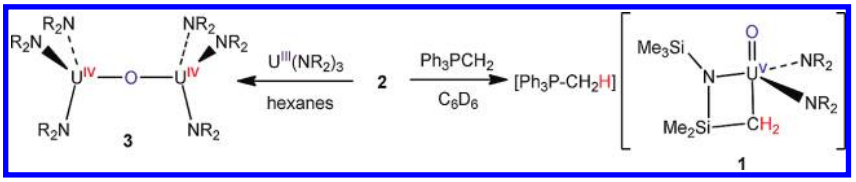

solution at very short reaction times, which could correspond to the putative TEMPO adduct, $U^{IV}(NR_2)_3$(TEMPO). In contrast, for the reaction of $U(NR_2)_3$ with Me_3NO, the relative rates are reversed. That is, Me_3NO coordination is slow (in part because of its poor solubility in pentane), whereas N−O bond cleavage is fast. As a result, $U(NR_2)_3(O)$ is generated in the presence of unconsumed $U(NR_2)_3$, resulting in the formation of complex **3** via conproportionation.

The electronic properties of **2** have been assessed by SQUID magnetometry. At 300 K, **2** exhibits an effective magnetic moment of 1.59 μ_B which gradually decreases upon cooling to 0.94 μ_B at 4 K, a temperature response characteristic of U(V) (Figure 2).[15] The μ_{eff} of **2** at room temperature is significantly lower than the theoretical U^{5+} free ion value (μ_{eff} = 2.54 μ_B) and surprisingly much lower than values found for the closely related U(V) oxo complexes **1** (μ_{eff} = 1.97 μ_B) and [U(O)-(tacn(OAr^R)$_3$)] (μ_{eff} = 1.98 μ_B, R = ^{t}Bu; μ_{eff} = 1.92 μ_B, R = Ad).[15] This low μ_{eff} value may be attributable to the quenching of spin−orbit coupling arising from covalent metal−ligand interactions.[15,34] We have also recorded the EPR spectrum of complex **2** (see Supporting Information, Figure S29). The spectrum reveals a highly anisotropic signal, in which $g_{\|}$ = 2.17 and $g_{\perp}$ < 0.7. Because we were only able to record a partial spectrum, we were limited in the amount of information that could be extracted. However, the observation of a signal does support the 5+ oxidation state assignment of this complex.

Complex **2** crystallizes in the monoclinic space group $P2_1/c$ (Figure 4). In the solid-state, **2** features a U−O_{oxo} bond length

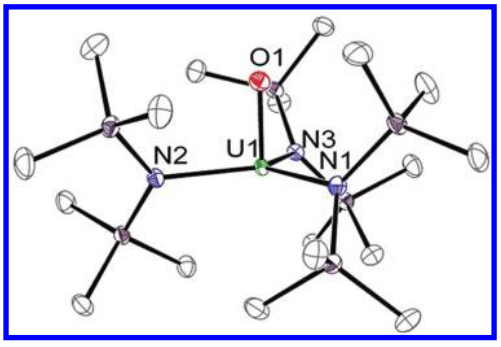

Figure 4. ORTEP diagram of $U(O)(NR_2)_3$ (R = $SiMe_3$) (**2**) with 50% probability ellipsoids. Hydrogen atoms omitted for clarity. Selected bond lengths (Å) and angles (deg): U1−O1 = 1.817(1), U1−N1 = 2.235(1), U1−N2 = 2.244(2), U1−N3 = 2.242(1), O1−U1−N1 = 92.53(6), O1−U1−N2 = 92.16(6), O1−U1−N3 = 92.48(5), N1−U1−N2 = 119.30(5), N1−U1−N3 = 118.16(5).

of 1.817(1) Å, comparable to the U═O bond lengths of **1** (U−O = 1.847(2) Å) and ((^{R}ArO)$_3$tacn)U(O) (U−O = 1.848(8) Å, R = ^{t}Bu; U−O = 1.848(4) Å, R = Ad).[15] Furthermore, **2** adopts a trigonal pyramidal geometry about the metal center (e.g., O1−U1−N1 = 92.53(6)°, N1−U1−N2 = 119.30(5)°) with its uranium atom lying only 0.0933(8) Å above the plane defined by the amide nitrogen atoms. This lies in stark contrast to the pyramidal molecular structure of $U(NR_2)_3$,[44] as well as the pseudotetrahedral geometries of complexes **3**, **4**, $U(H)(NR_2)_3$,[45] and the group 4 tris(silylamide) complexes $MCl(NR_2)_3$ (M = Ti, Zr, Hf).[46] Moreover, the structures of the closely related U(V) imido complex $U(═NR)(NR_2)_3$[47] and the Nb(V) oxo complex $Nb(O)(NR_2)_3$ are also pseudotetrahedral.[48] In the niobium example, the niobium atom is positioned 0.416 Å above the plane defined by the nitrogen atoms. Taken together, this structural data suggests that the tris(silylamide) framework can easily adopt a pseudotetrahedral coordination environment. As such, the trigonal pyramidal geometry of **2** is highly unusual, suggesting that its structure may be imposed by electronic effects that exceed both the electrostatic and the steric demands of the coligands. Accordingly, we returned to DFT to probe this, and other aspects, of **2**.

The optimized geometry of **2** agrees very well with the experimental structural data. The computed U−O and average U−N distances are slightly longer than experiment, at 1.838 Å and 2.267 Å, respectively and, pleasingly, calculation agrees with experiment in finding a trigonal pyramidal geometry, with O−U−N angles of 89.4°, 91.7° and 89.1°, and N−U−N angles of 118.3°, 123.7° and 118.3°.

As expected for a U(V) complex, the singly occupied molecular orbital (SOMO) is a U 5f-based electron (Table 1). The

Table 1. Compositions (Mulliken Analysis, Threshold = 1%) and Energies (eV) of Selected Canonical α Spin Orbitals of $U(O)(NR_2)_3$ (2)

orbital	energy	5f	6d	7p	total O	total N	principal bonding character
SOMO	−3.891	93.8					unpaired e$^-$
HOMO-1	−5.756	4.8			2.6	54.6	N lone pair
HOMO-2	−5.809	4.9			1.8	53.1	N lone pair
HOMO-3	−5.853	11.0			2.3	46.5	N lone pair
HOMO-13	−7.538	6.7	7.3	2.5	36.2	2.1	U−O σ
HOMO-14	−7.633	8.9	2.7		41.0	2.2	U−O π
HOMO-15	−7.659	8.5	2.8		40.8	1.1	U−O π

SOMO is shown in Figure 5, together with three other orbitals which, although rather delocalized, clearly demonstrate U−O covalent bonding. The U−O bonding orbitals are polarized toward the oxygen, but also possess significant metal character. The Gopinathan−Jug U−O bond order is calculated to be 2.34,[49] very similar to that found for the analogous bond in **1** (2.29).[20] The Mulliken charge of the uranium is +1.93 in **2**, in comparison with +1.85 in **3**, consistent with the increase in formal oxidation state.

Directly below the SOMO come six orbitals with nitrogen character. HOMO-4 to HOMO-6 are very delocalized, with only about 25% nitrogen content, but HOMO-1 to HOMO-3 are much more nitrogen-based. They are shown in Figure 6, together with the analogous orbitals following Boys−Foster[50] localization of the canonical Kohn−Sham levels. The localized orbitals are about 80% nitrogen in content, and display U−N bonding character.

dx.doi.org/10.1021/ic201936j | Inorg. Chem. 2012, 51, 1625−1633

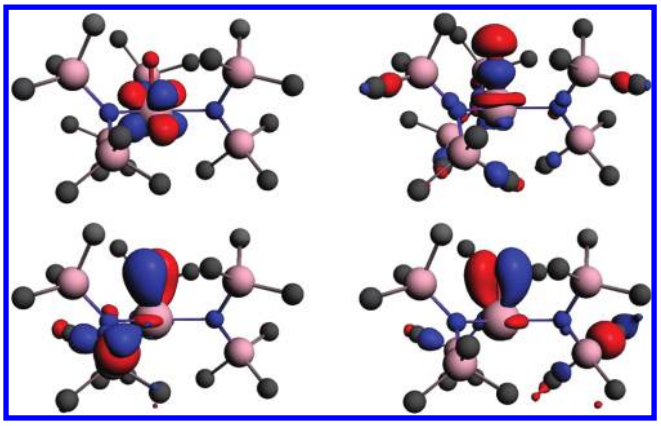

Figure 5. Representations of (clockwise from top left) the α spin 93a (SOMO), 80a (HOMO-13), 79a (HOMO-14), and 78a (HOMO-15) molecular orbitals of **2**. The isosurface level is 0.05 in all cases. H atoms omitted for clarity.

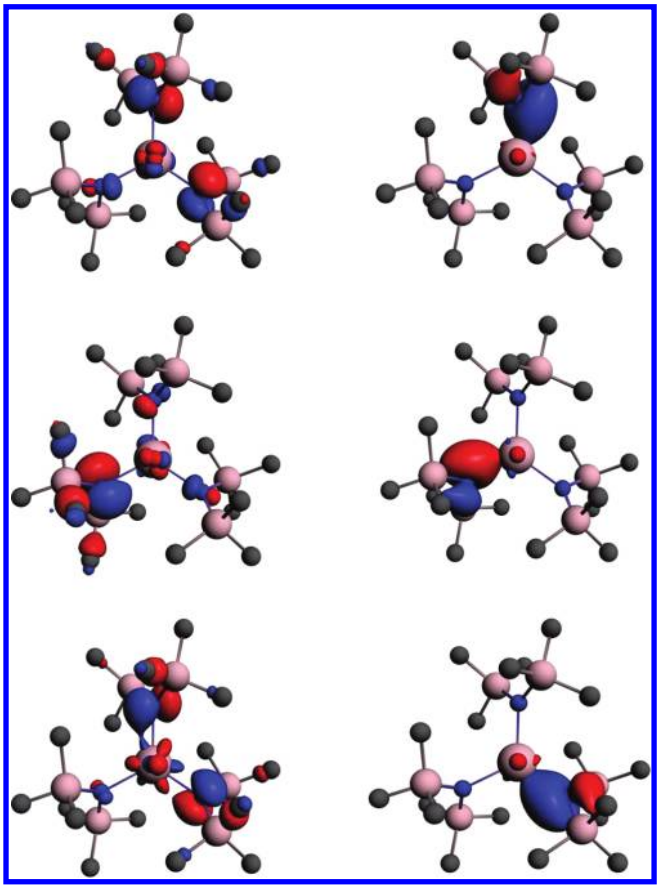

Figure 6. Representations of (left column) the α spin 92a (HOMO-1), 91a (HOMO-2), and 90a (HOMO-3) molecular orbitals of **2** (viewed down the U−O vector), and (right column) the analogous orbitals following Boys−Foster localization. The isosurface level is 0.05 in all cases. H atoms omitted for clarity.

To probe the origin of the trigonal planar geometry, we performed a series of constrained geometry optimizations (lineartransit) in which the three O−U−N angles were set equal to one another and simultaneously altered from 90° to 110° in steps of 2°, allowing all other geometric variables to relax at each step. The total molecular energy becomes gradually less negative during the course of this distortion, with the 110° structure being 35.1 kJ·mol^{-1} less stable than that at 90°, as shown in Figure 7 (top). The U−O and average U−N bond lengths increase by only 0.007 Å over this distortion, clearly demonstrating

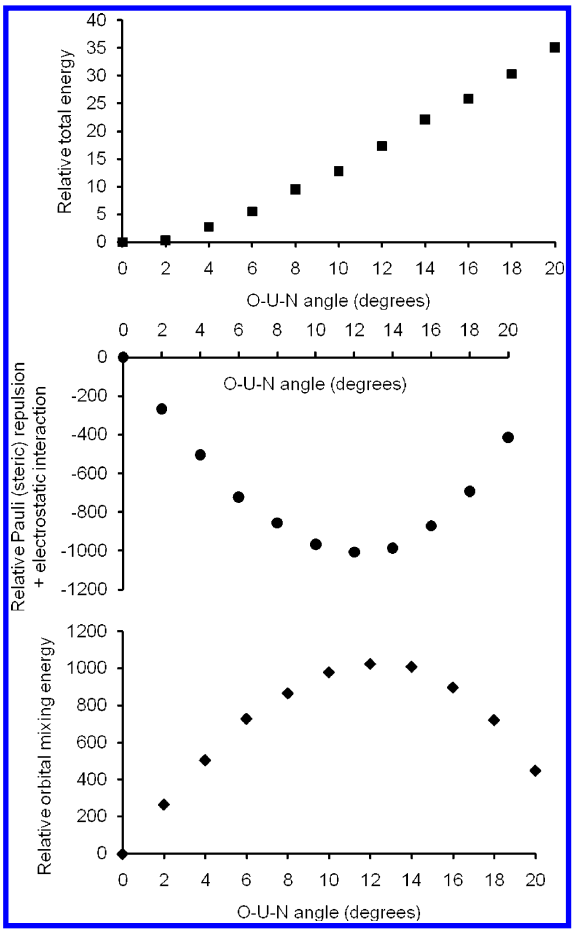

Figure 7. Changes in the total energy, sum of the prerelaxation Pauli repulsion and electrostatic energies, and orbital mixing energies (kJ·mol^{-1}) in **2** as a function of O−U−N angle (shown as values in excess of 90°), relative to the values at 90°.

that the energy change does not result from significant alterations in the lengths of the bonds to the metal center.

At each step of the lineartransit we have decomposed the total molecular energy using the Ziegler−Rauk scheme.[51,52] The changes in the pre-SCF relaxation electrostatic energy term are approximately a factor of 10 smaller than the changes in the pre-SCF relaxation Pauli (steric) repulsion and post-SCF relaxation orbital mixing energies. Figure 7 shows the changes in the orbital mixing term throughout the distortion, together with the sum of the pre-SCF relaxation electrostatic and Pauli interactions. As might be expected, increasing the O−U−N angle from 90° causes the sum of the pre-SCF relaxation terms to become more favorable as the ligands move apart from each other and the geometry approaches pseudotetrahedral. Toward the end of the distortion, however, the pre-SCF relaxation term becomes more positive once again, presumably as a result of increasing repulsive interactions between the bulky $N(SiMe_3)_2$ ligands. The orbital mixing term shows the opposite trend to the pre-SCF relaxation terms, that is, the most negative (stabilizing) value of this contribution to the total energy comes at 90°. We therefore conclude that the origin of the trigonal pyramidal geometry of **2** lies in the orbital mixing term, although the requirement to run

dx.doi.org/10.1021/ic201936j | Inorg. Chem. 2012, 51, 1625−1633

the lineartransit calculations without symmetry constraints precludes further analysis of the orbital interaction energy.

Eisenstein et al. have invoked a second order Jahn−Teller mechanism to explain the pseudo C_{3v} geometries of trigonal complexes of the lanthanides.[53,54] In this explanation, C_{3v}-like structures are favored over planar D_{3h} through enhanced bonding as a result of mixing between metal 5d (for Ln) or 6d (for An) orbitals and ligand levels, which is symmetry forbidden in the planar geometry. Evidence for this mechanism comes in the form of enhanced orbital mixing and metal orbital populations in the pseudo C_{3v} structures.

Table 2 presents the uranium Mulliken atomic populations and atomic orbital character of the HOMO-1−HOMO-3 of **2** at the start of the lineartransit and at the point at which the orbital mixing term is least negative (i.e., at an O−U−N angle of 102°). With the exception of the p population, all the other uranium populations are smaller at the larger angle, as is the uranium contribution to the three metal−nitrogen orbitals. These observations are consistent with the reduced orbital mixing energy found in the Ziegler−Rauk breakdown, and suggest that there is no second order Jahn−Teller driver toward increased O−U−N angles in **2**.

Table 2. Mulliken Atomic Populations (e^-) of Uranium and Average U and N Content of the N-based Canonical α Spin Orbitals of $U(O)(NR_2)_3$ (2)

O−U−N angle (deg)	U s	U p	U d	U f	% U in HOMO-1−HOMO-3 (av.)	% N in HOMO-1−HOMO-3 (av.)
90	2.187	5.685	1.582	2.616	6.9	51.4
102	2.161	5.715	1.573	2.569	5.3	51.9

SUMMARY

We have demonstrated that addition of Me_3NO to $U(NR_2)_3$ does not produce the terminal oxo complex $U(O)(NR_2)_3$ as originally reported,[24] but instead generates the U(IV) bridging oxo $[(NR_2)_3U]_2(\mu\text{-}O)$. In contrast, treatment of $U(NR_2)_3$ with TEMPO readily affords $U(O)(NR_2)_3$ in good yield. This complex is marked by a trigonal pyramidal geometry in the solid-state. The short U═O bond found for $U(O)(NR_2)_3$ suggests a covalent U═O interaction leading to electronic control of the geometry. DFT calculations support this assertion not only by identifying covalent bonding within the U−O σ and π molecular orbitals but also, via energy decomposition analysis, by demonstrating that the adoption of the trigonal pyramidal geometry is orbitally driven. For future work we intend to further examine the chemistry of $U(O)(NR_2)_3$ and the reactivity of its oxo group.

EXPERIMENTAL SECTION

General Information. All reactions and subsequent manipulations were performed under anaerobic and anhydrous conditions under an atmosphere of argon or nitrogen. Diethyl ether, tetrahydrofuran (THF), and hexane were dried using a Vacuum Atmospheres DRI-SOLV Solvent Purification system. Pentane and CH_2Cl_2 were dried over activated 4 Å and 3 Å molecular sieves, respectively, for 24 h prior to use. All deuterated solvents were purchased from Cambridge Isotope Laboratories Inc. and were dried over activated 4 Å molecular sieves for 24 h prior to use. $U[N(SiMe_3)_2]_3$[24] and Ph_3PCH_2[55] were synthesized according to published procedures. $U[N(SiMe_3)_2]_3$ was purified by recrystallization from hexane or sublimation at 110 °C under reduced pressure. When isolated by sublimation the yield of $U[N(SiMe_3)_2]_3$ was 56%. All other reagents were obtained from commercial sources and used as received.

NMR spectra were recorded on a Varian UNITY INOVA 500 spectrometer. ^1H NMR spectra are referenced to $SiMe_4$ using the residual protio solvent peaks as internal standards. $^{31}P\{^1H\}$ NMR spectra were referenced to external 85% H_3PO_4. Elemental analyses were performed by the Micro-Mass Facility at the University of California, Berkeley. UV−vis/NIR spectra were recorded on a UV-3600 Shimadzu spectrophotometer. IR data were collected using a Nicolet 6700 FT-IR spectrometer. Electron paramagnetic resonance spectra were obtained at 8 K using a Varian E-12 spectrometer equipped with an Oxford liquid He cryostat, an EIP-547 microwave frequency counter, and a Varian E-500 gaussmeter, which was calibrated using 2,2-diphenyl-1-picrylhydrazyl (DPPH, g = 2.0036).

Magnetism Measurements. Magnetism data were recorded using a Quantum Design MPMS 5XL SQUID magnetometer. The experiments were performed between 4−300 K using 50−100 mg of powdered, crystalline solid. The solids were loaded into an NMR tube, which was subsequently flame-sealed. The solids were kept in place with approximately 100 mg of quartz wool packed on either side of the sample. The data was corrected for the contribution of the NMR tube holder and the quartz wool. The experiments were performed using a 0.5 T field. Diamagnetic corrections ($\chi_{dia} = -3.99 \times 10^{-4}$ cm^3·mol^{-1} for **2**; $\chi_{dia} = -8.04 \times 10^{-4}$ cm^3·mol^{-1} for **3**; $\chi_{dia} = -4.38 \times 10^{-4}$ cm^3·mol^{-1} for **4**) were made using Pascal's constants.[56]

Synthesis of $U(O)[N(SiMe_3)_2]_3$ (2). To a cold (−25 °C) stirring solution of $U[N(SiMe_3)_2]_3$ (0.518 g, 0.720 mmol) in hexane (5 mL) was added a cold (−25 °C) solution of TEMPO (0.113 g, 0.723 mmol) in hexane (2 mL) dropwise. Upon addition, the solution immediately turned pale orange in color. Within seconds, however, this orange solution converted to a dark red color. After stirring for 5 min at room temperature, the volume of the solution was reduced by half in vacuo. Storage of the solution at −25 °C for 24 h resulted in the deposition of red crystalline material, 0.384 g, 73% yield. ^1H NMR (500 MHz, 25 °C, C_6D_6): δ −0.23 (s, 54H, NSiMe_3). Anal. Calcd for $C_{18}H_{54}N_3OSi_6U$: C, 29.40; H, 7.42; N, 5.72. Found: C, 29.57; H, 7.39; N, 5.47. UV−vis/NIR (C_7H_8, 14.3 mM, 25 °C, L·mol^{-1}·cm^{-1}): 1016 (ε = 54.4), 1116 (ε = 32.6), 1254 (ε = 80.1), 1662 (overlap with solvent absorption). IR (KBr pellet, cm^{-1}): 2960 (m), 2950 (m), 2897 (w), 2362 (w), 2337(w), 1923 (w), 1845 (w), 1431 (w), 1416 (w), 1401 (w), 1250 (s), 1182 (w), 930 (s), 840 (s), 816 (sh m), 767 (s), 729 (w), 682 (w), 672 (w), 650 (m), 609 (s). Melting point: 104−105 °C (dec.).

Reaction of $U[N(SiMe_3)_2]_3$ with TEMPO in the Presence of 9,10-Dihydroanthracene. To a deep purple solution of $U[N(SiMe_3)_2]_3$ (0.020 g, 0.028 mmol) in C_6D_6 (0.7 mL) was added 9,10-dihydroanthracene (0.007 g, 0.039 mmol). TEMPO (0.004 g, 0.026 mmol) was subsequently added to the deep purple reaction mixture resulting in formation of a red solution. A ^1H NMR spectrum of the solution revealed the presence of **2**, 2,2,6,6-tetramethylpiperidine, 9,9′,10,10′-tetrahydro-9,9′-bianthracene, and unreacted 9,10-dihydroanthracene. The presence of 2,2,6,6-tetramethylpiperidine in the product mixture was confirmed by comparison of its spectral properties to a solution of commercially obtained 2,2,6,6-tetramethylpiperidine in C_6D_6. The presence of 9,9′,10,10′-tetrahydro-9,9′-bianthracene in the product mixture was confirmed by comparison of the resonances to reported values.[57]

Synthesis of $[(N(SiMe_3)_2)_3U]_2(\mu\text{-}O)$ (3) from $U(NR_2)_3$ and 0.5 equiv of Me_3NO. To a solution of $U[N(SiMe_3)_2]_3$ (0.103 g, 0.143 mmol) in pentane (2 mL) was added Me_3NO (0.006 g, 0.080 mmol). The reaction mixture gradually turned dark brown-red. After 1 h the volatiles were removed in vacuo and the solid was dissolved in toluene (8 mL). The resulting solution was filtered through a Celite column (2 cm ×0.5 cm) supported on glass wool. Storage of the filtrate at −25 °C for 24 h resulted in the deposition of light yellow crystals. 0.055 g, 53% yield. The crystals of **3** used for X-ray crystallography were grown from a dilute C_6D_6 solution over 4 d at room temperature, affording the solvate **3**·2.5C_6D_6. ^1H NMR (500 MHz, 25 °C, C_7D_8): δ −28.64 (br s, 18H, fwhm = 1300 Hz, NSiMe_3), −16.79 (br s, 18H, fwhm = 1300 Hz, NSiMe_3), and −6.50 (br s, 18H, fwhm = 1300 Hz, NSiMe_3), 15.23 (br s, 54H, fwhm = 2300 Hz, NSiMe_3). ^1H NMR

dx.doi.org/10.1021/ic201936j | Inorg. Chem. 2012, 51, 1625−1633

(500 MHz, −3 °C, C_7D_8): δ −32.38 (s, 18H, NSi*Me*$_3$), −19.52 (s, 18H, NSi*Me*$_3$), −7.57 (s, 18H, NSi*Me*$_3$), 8.76 (br s, 54 H, fwhm = 19,000 Hz, NSi*Me*$_3$). ^{1}H NMR (500 MHz, −13 °C, C_7D_8): δ −34.07 (s, 18H, NSi*Me*$_3$), −20.36 (s, 18H, NSi*Me*$_3$), −8.11 (s, 18H, NSi*Me*$_3$), resonances assignable to 54 silylamide methyl protons not observed. ^{1}H NMR (500 MHz, −26 °C, C_7D_8): δ −36.30 (s, 18H, NSi*Me*$_3$), −21.96 (s, 18H, NSi*Me*$_3$), −8.56 (s, 18H, NSi*Me*$_3$), resonances assignable to 54 silylamide methyl protons not observed. ^{1}H NMR (500 MHz, −41 °C, C_7D_8): δ −39.76 (s, 18H, NSi*Me*$_3$), −24.30 (s, 18H, NSi*Me*$_3$), −19.42 (br s, 18H, fwhm = 2500 Hz, NSi*Me*$_3$), −9.56 (s, 18H, NSi*Me*$_3$), 14.32 (br s, 18H, fwhm = 2500 Hz, NSi*Me*$_3$), 71.99 (br s, 18H, fwhm = 3000 Hz, NSi*Me*$_3$). ^{1}H NMR (500 MHz, −55 °C, C_7D_8): δ −43.23 (s, 18H, NSi*Me*$_3$), −26.79 (s, 18H, NSi*Me*$_3$), −22.98 (br s, 18H, fwhm = 900 Hz, NSi*Me*$_3$), −10.53 (s, 18H, NSi*Me*$_3$), 14.21 (br s, 18H, fwhm = 900 Hz, NSi*Me*$_3$), 80.61 (br s, 18H, fwhm = 900 Hz, NSi*Me*$_3$). ^{1}H NMR (500 MHz, 45 °C, C_7D_8): δ −14.05 (br s, 54H, fwhm = 5000 Hz, NSi*Me*$_3$), 13.49 (br s, 54H, fwhm = 2000 Hz, NSi*Me*$_3$). Anal. Calcd for $C_{36}H_{108}N_6OSi_{12}U$: C, 29.73; H, 7.50; N, 5.78. Found: C, 29.87; H, 7.46; N, 5.59. UV−vis/NIR (C_7H_8, 4.7 mM, 25 °C, L·mol^{-1}·cm^{-1}): 516 (ε = 34.2), 574 (ε = 15.5), 646 (ε = 11.3), 686 (ε = 89.5), 848 (ε = 12.6), 880 (ε = 10.0), 1076 (ε = 25.5), 1168 (ε = 34.1), 1420 (ε = 14.3), 1578 (ε = 21.7), 1772 (ε = 23.4). IR (KBr pellet, cm^{-1}): 2960 (sh m), 2955 (m), 2901 (m), 1629 (w), 1432 (w), 1405 (w), 1249 (s), 1182 (w), 932 (m), 882 (s), 848 (s), 836 (sh s), 774 (m), 760 (m), 707 (w), 682 (m), 659 (m), 632 (w), 613 (m), 463 (m). Complex **3** exhibits an effective magnetic moment of 3.84 μ_B at 300 K, which decreases to 1.33 μ_B at 4 K. Melting point: 155−157 °C.

Synthesis of [(N(SiMe$_3$)$_2$)$_3$U]$_2$(μ-O) (3) from U(NR$_2$)$_3$ and 1 equiv of Me$_3$NO. To a solution of U[N(SiMe$_3$)$_2$]$_3$ (0.099 g, 0.138 mmol) in pentane (2 mL) was added Me$_3$NO (0.011 g, 0.146 mmol). The reaction mixture gradually turned dark brown-red. After 2 h the volatiles were removed in vacuo affording a dark brown solid. The solid was washed with hexanes (3 × 2 mL) providing a light yellow powder. The powder was dissolved in THF (6 mL) and the pale yellow solution was filtered through a Celite column (2 cm ×0.5 cm) supported on glass wool. Storage of the filtrate at −25 °C for 24 h resulted in the deposition of light yellow crystals. 0.033 g, 33% yield.

Synthesis of [(N(SiMe$_3$)$_2$)$_3$U]$_2$(μ-O) (3) from U[N(SiMe$_3$)$_2$]$_3$ and 2. To a stirring solution of U[N(SiMe$_3$)$_2$]$_3$ (0.065 g, 0.090 mmol) in toluene (5 mL) was added dropwise a solution of **2** (0.066 g, 0.090 mmol) in toluene (5 mL). Upon addition, the solution immediately turned light yellow in color. Storage of the solution at −25 °C for 24 h resulted in the deposition of light yellow crystalline material, which was collected by decanting the supernatant (0.053 g). Concentration and storage of the supernatant for 24 h at −25 °C resulted in the further deposition of yellow crystals (0.040 g). Total: 0.093 g, 71% yield.

Synthesis of U(I)[N(SiMe$_3$)$_2$]$_3$ (4). To a stirring solution of U[N(SiMe$_3$)$_2$]$_3$ (0.270 g, 0.375 mmol) in hexanes (3 mL) was added dropwise a solution of I_2 (0.045 g, 0.176 mmol) in Et_2O (2 mL). Upon addition, a nearly colorless microcrystalline precipitate formed. This solid was isolated by decanting off the supernatant. The material was subsequently dissolved in CH_2Cl_2 (16 mL) and filtered through a Celite column (2 cm ×0.5 cm) supported on glass wool. Storage of the solution at −25 °C for 24 h resulted in the deposition of light tan crystalline blocks; 0.199 g, 62% yield. The crystals of **4** used for X-ray crystallography were grown by storage of dilute hexane/Et_2O solution at −25 °C for 24 h. $C_{18}H_{54}N_3ISi_6U$: C, 25.55; H, 6.43; N, 4.97. Found: C, 25.31; H, 6.58; N, 4.86. ^{1}H NMR (500 MHz, 25 °C, C_6D_6): δ −0.98 (s, 54H, NSi*Me*$_3$). UV−vis/NIR (THF, 9.8 mM, 25 °C, L·mol^{-1}·cm^{-1}): 452 (sh, ε = 14.0), 495 (ε = 13.0), 520 (ε = 18.7), 524 (ε = 15.6), 554 (sh, ε = 7.6), 608 (ε = 6.6), 640 (sh, ε = 6.5), 660 (sh, ε = 10.9), 688 (ε = 21.7), 796 (ε = 5.6), 882 (ε = 3.7), 940 (ε = 4.9), 1034 (ε = 20.9), 1050 (ε = 20.8), 1340 (ε = 14.5), 1532 (ε = 10.1). IR (KBr pellet, cm^{-1}): 2956 (m), 2898 (m), 1592 (w), 1408 (w), 1251 (s), 1182 (w), 1072 (w), 983 (sh w), 921 (sh m), 891 (s), 847 (s), 770 (m), 755 (m), 678 (w), 656 (w), 613 (m). Complex **4** exhibits an effective magnetic moment of 3.35 μ_B at 300 K which decreases to 2.16 μ_B at 4 K.

Reaction of U[N(SiMe$_3$)$_2$]$_3$ with Me$_3$NO in the Presence of NaI. To a deep purple solution of U[N(SiMe$_3$)$_2$]$_3$ (0.035 g, 0.049 mmol) in hexane (2 mL) was added THF (50 μL) and finely ground NaI (0.007 g, 0.047 mmol). The solution was stirred for 30 min at room temperature, whereupon Me$_3$NO (0.002 g, 0.027 mmol) was added. After 1 h of stirring, the solution became brown-orange in color. The volatiles were removed in vacuo, and the crude solid was dissolved in C_6D_6 and analyzed by ^{1}H NMR spectroscopy (see the Supporting Information). The presence of U(I)[N(SiMe$_3$)$_2$]$_3$ in the product mixture was confirmed by comparison with a spectrum of an independently prepared sample of **4**. NOTE: NaI and Me$_3$NO are not observed to react with each other under these reaction conditions.

Synthesis of [Ph$_3$PCH$_3$][U(O)(*CH*$_2$SiMe$_2$*N*SiMe$_3$)(NR$_2$)$_2$] (R = SiMe$_3$) (1) from the reaction of 2 with Ph$_3$PCH$_2$. An NMR tube equipped with a J-Young valve was charged with a solution of **2** (0.012 g, 0.016 mmol) in C_6D_6 (0.7 mL) to which Ph_3PCH_2 (0.005 g, 0.018 mmol) was added. Upon addition, the deep red solution immediately turned red-brown in color. Analysis of the solution by ^{1}H and ^{31}P{^{1}H} NMR revealed the formation of [Ph_3PCH_3][U(O)(CH$_2$SiMe$_2$*N*SiMe$_3$)(NR$_2$)$_2$] as indicated by comparison of the spectra to independently prepared material.[20] ^{1}H NMR (500 MHz, 25 °C, C_6D_6): δ −6.00 (s, 36H, NSi*Me*$_3$), −4.09 (s, 9H, CH$_2$SiMe$_2$NSi*Me*$_3$), 8.38 (s, 3H, *p*-aryl CH), 8.97 (s, 6H, aryl CH), 9.20 (s, 6H, aryl CH), 14.13 (s, 6H, CH$_2$Si*Me*$_2$NSiMe$_3$), 16.01 (s, 3H, Ph_3PCH_3), 36.71 (br s, 2H, *CH*$_2$SiMe$_2$NSiMe$_3$). ^{31}P{^{1}H} NMR (202 MHz, 25 °C, C_6D_6): δ 30.28 (s).

X-ray Crystallography. Data for **2** and **3**·2.5C_6D_6 were collected on a Bruker KAPPA APEX II diffractometer equipped with an APEX II CCD detector using a TRIUMPH monochromator with a Mo Kα X-ray source (α = 0.71073 Å), while the data was for **4** was collected on a Bruker 3-axis platform diffractometer equipped with a SMART-1000 CCD detector using a graphite monochromator with a Mo Kα X-ray source (α = 0.71073 Å). The crystals of **2** and **3**·2.5C_6D_6 were mounted on a cryoloop under Paratone-N oil, and all data were collected at 100(2) K using an Oxford nitrogen gas cryostream system. The crystal of **4** was mounted on a glass fiber under Paratone-N oil, and all data were collected at 150(2) K using an Oxford nitrogen gas cryostream system. A hemisphere of data was collected using ω scans with 0.5° frame widths. Frame exposures of 5, 10, and 15 s were used for **2**, **3**·2.5C_6D_6, and **4**, respectively. Data collection and cell parameter determination were conducted using the SMART program.[58] Integration of the data frames and final cell parameter refinement were performed using SAINT software.[59] Absorption correction of the data for **2** and **3**·2.5C_6D_6 was carried out using SADABS,[60] while the absorption correction of the data for **4** was carried out empirically based on reflection ψ-scans. Subsequent calculations were carried out using SHELXTL.[61] Structure determination was done using direct or Patterson methods and difference Fourier techniques. All hydrogen atom positions were idealized and rode on the atom of attachment. Structure solution, refinement, graphics, and creation of publication materials were performed using SHELXTL.[61]

Complex **3**·2.5C_6D_6 contains two disordered C_6D_6 molecules. Each disordered C_6D_6 molecule was modeled over two positions with 50:50 occupancies. The carbon atoms of the C_6D_6 molecules were not refined anisotropically and hydrogen atoms were not assigned to these carbons. A summary of relevant crystallographic data for complexes **2**, **3**·2.5C_6D_6, and **4** is presented in Table 3.

Computational Details. Spin-unrestricted, gradient corrected DFT calculations were carried out using the PBE functional,[62,63] as implemented in the Amsterdam Density Functional 2010.02[64,65] code. The Zeroth Order Regular Approximation (ZORA) Hamiltonian was employed in all calculations. Slater Type Orbital ZORA basis sets of DZP quality were used for all atoms except U, for which a TZP ZORA basis set was employed. The frozen core approximation was employed for all atoms except H; C(1s), N(1s), O(1s), Si(2p), U(5d). The geometry of **2** was optimized without symmetry constraints, and that of **3** within the D_3 point group, using the default self consistent field (SCF) and geometry convergence criteria, together with an integration grid of 4.5. Ziegler−Rauk bond energy decomposition analysis was performed.[51,52] Gopinathan−Jug bond orders were also computed.[49]

dx.doi.org/10.1021/ic201936j | Inorg. Chem. 2012, 51, 1625−1633

Table 3. X-ray Crystallographic Data for 2, 3·2.5C_6D_6, and 4

	2	3·2.5C_6D_6	4
empirical formula	$C_{18}H_{54}N_3OSi_6U$	$C_{51}H_{123}N_6OSi_{12}U_2$	$C_{18}H_{54}IN_3Si_6U$
crystal habit, color	block, red	block, yellow	block, tan
crystal size (mm)	0.20 × 0.20 × 0.20	0.21 × 0.16 × 0.15	0.30 × 0.30 × 0.10
crystal system	monoclinic	monoclinic	trigonal
space group	$P2_1/c$	$C2/c$	$R3c$
volume (Å^3)	3263.4(1)	30929(1)	5008.9(3)
a (Å)	12.4187(3)	30.8900(7)	18.2954(5)
b (Å)	18.1898(4)	19.9441(4)	18.2954(5)
c (Å)	14.8632(4)	50.226(1)	17.280(1)
α (deg)	90	90	90
β (deg)	103.600(1)	91.699(1)	90
γ (deg)	90	90	120
Z	4	16	6
formula weight (g/mol)	735.21	1649.69	846.11
density (calculated) (Mg/m^3)	1.496	1.417	1.683
absorption coefficient (mm^{-1})	5.208	4.404	6.012
F_{000}	1468	13296	2472
total no. reflections	34039	104426	7595
unique reflections	12424	29399	2291
final R indices ($I > 2\sigma(I)$]	R_1 = 0.0220	R_1 = 0.0614	R_1 = 0.0281
	wR_2 = 0.0433	wR_2 = 0.1149	wR_2 = 0.0803
largest diff. peak and hole (e$^-$ Å^{-3})	1.355 and −0.931	2.534 and −5.483	1.567 and −1.072
GOF	1.009	1.079	1.079

■ ASSOCIATED CONTENT

Supporting Information

Experimental procedures, crystallographic details (as CIF files), and spectral data for **2**–**4**; optimized Cartesian coordinates for **2** and **3**. This material is available free of charge via the Internet at http://pubs.acs.org.

■ AUTHOR INFORMATION

Corresponding Author

*E-mail: hayton@chem.ucsb.edu (T.W.H.), n.kaltsoyannis@ucl.ac.uk (N.K.).

■ ACKNOWLEDGMENTS

We thank the University of California, Santa Barbara, and the Department of Energy (BES Heavy Element Program) for financial support of this work. We are grateful to UCL for computing resources via the Research Computing "Legion" cluster and associated services, and the U.K. EPSRC for computing resources under grant GR/S06233 and via its National Service for Computational Chemistry Software (http://www.nsccs.ac.uk). We also thank Wayne W. Lukens, Jr. (LBNL) for recording the EPR spectrum of **2**.

■ REFERENCES

(1) Fortier, S.; Hayton, T. W. *Coord. Chem. Rev.* **2010**, *254*, 197–214.
(2) Denning, R. G. *Struct. Bonding (Berlin)* **1992**, *79*, 215–276.
(3) Denning, R. G. *J. Phys. Chem. A* **2007**, *111*, 4125–4143.
(4) Hayton, T. W. *Dalton Trans.* **2010**, *39*, 1145–1158.
(5) Zi, G.; Jia, L.; Werkema, E. L.; Walter, M. D.; Gottfriedsen, J. P.; Andersen, R. A. *Organometallics* **2005**, *24*, 4251–4264.
(6) Lam, O. P.; Heinemann, F. W.; Meyer, K. *Chem. Sci.* **2011**, *2*, 1538–1547.
(7) Lam, O. P.; Bart, S. C.; Kameo, H.; Heinemann, F. W.; Meyer, K. *Chem. Commun.* **2010**, *46*, 3137–3139.
(8) Avens, L. R.; Barnhart, D. M.; Burns, C. J.; McKee, S. D.; Smith, W. H. *Inorg. Chem.* **1994**, *33*, 4245–4254.
(9) Kraft, S. J.; Walensky, J.; Fanwick, P. E.; Hall, M. B.; Bart, S. C. *Inorg. Chem.* **2010**, *49*, 7620–7622.
(10) Arney, D. S. J.; Burns, C. J. *J. Am. Chem. Soc.* **1995**, *117*, 9448–9460.
(11) Arney, D. S. J.; Burns, C. J. *J. Am. Chem. Soc.* **1993**, *115*, 9840–9841.
(12) Evans, W. J.; Kozimor, S. A.; Ziller, J. W. *Polyhedron* **2004**, *23*, 2689–2694.
(13) Gardner, B. M.; Lewis, W.; Blake, A. J.; Liddle, S. T. *Inorg. Chem.* **2011**, *50*, 9631–9641.
(14) Barros, N.; Maynau, D.; Maron, L.; Eisenstein, O.; Zi, G.; Andersen, R. A. *Organometallics* **2007**, *26*, 5059–5065.
(15) Bart, S. C.; Anthon, C.; Heinemann, F. W.; Bill, E.; Edelstein, N. M.; Meyer, K. *J. Am. Chem. Soc.* **2008**, *130*, 12536–12546.
(16) Castro-Rodriguez, I.; Meyer, K. *J. Am. Chem. Soc.* **2005**, *127*, 11242–11243.
(17) Lam, O. P.; Anthon, C.; Meyer, K. *Dalton Trans.* **2009**, 9677–9691.
(18) Karmazin, L.; Mazzanti, M.; Pecaut, J. *Inorg. Chem.* **2003**, *42*, 5900–5908.
(19) Lukens, W. W.; Beshouri, S. M.; Blosch, L. L.; Andersen, R. A. *J. Am. Chem. Soc.* **1996**, *118*, 901–902.
(20) Fortier, S.; Kaltsoyannis, N.; Wu, G.; Hayton, T. W. *J. Am. Chem. Soc.* **2011**, *133*, 14224–14227.
(21) Lippert, C. A.; Soper, J. D. *Inorg. Chem.* **2010**, *49*, 3682–3684.
(22) Lucarini, M.; Marchesi, E.; Pedulli, G. F.; Chatgilialoglu, C. *J. Org. Chem.* **1998**, *63*, 1687–1693.
(23) Evans, W. J.; Perotti, J. M.; Doedens, R. J.; Ziller, J. W. *Chem. Commun.* **2001**, 2326–2327.
(24) Andersen, R. A. *Inorg. Chem.* **1979**, *18*, 1507–1509.
(25) Graves, C. R.; Kiplinger, J. L. *Chem. Commun.* **2009**, 3831–3853.
(26) Graves, C. R.; Vaughn, A. E.; Schelter, E. J.; Scott, B. L.; Thompson, J. D.; Morris, D. E.; Kiplinger, J. L. *Inorg. Chem.* **2008**, *47*, 11879–11891.
(27) Graves, C. R.; Scott, B. L.; Morris, D. E.; Kiplinger, J. L. *Organometallics* **2008**, *27*, 3335–3337.
(28) Graves, C. R.; Yang, P.; Kozimor, S. A.; Vaughn, A. E.; Clark, D. L.; Conradson, S. D.; Schelter, E. J.; Scott, B. L.; Thompson, J. D.; Hay, P. J.; Morris, D. E.; Kiplinger, J. L. *J. Am. Chem. Soc.* **2008**, *130*, 5272–5285.
(29) Graves, C. R.; Scott, B. L.; Morris, D. E.; Kiplinger, J. L. *J. Am. Chem. Soc.* **2007**, *129*, 11914–11915.
(30) Benaud, O.; Berthet, J.-C.; Thuery, P.; Ephritikhine, M. *Chem. Commun.* **2011**, *47*, 9057–9059.
(31) Cooper, O. J.; Mills, D. P.; McMaster, J.; Moro, F.; Davies, E. S.; Lewis, W.; Blake, A. J.; Liddle, S. T. *Angew. Chem., Int. Ed.* **2011**, *50*, 2383–2386.
(32) Roussel, P.; Boaretto, R.; Kingsley, A. J.; Alcock, N. W.; Scott, P. *Dalton. Trans.* **2002**, 1423–1428.
(33) Castro-Rodriguez, I.; Olsen, K.; Gantzel, P.; Meyer, K. *Chem. Commun.* **2002**, 2764–2765.
(34) Castro-Rodriguez, I.; Olsen, K.; Gantzel, P.; Meyer, K. *J. Am. Chem. Soc.* **2003**, *125*, 4565–4571.
(35) Schelter, E. J.; Yang, P.; Scott, B. L.; Thompson, J. D.; Martin, R. L.; Hay, P. J.; Morris, D. E.; Kiplinger, J. L. *Inorg. Chem.* **2007**, *46*, 7477–7488.
(36) Fortier, S.; Melot, B. C.; Wu, G.; Hayton, T. W. *J. Am. Chem. Soc.* **2009**, *131*, 15512–15521.

(37) Dormond, A.; El Bouadili, A.; Aaliti, A.; Moise, C. *J. Organomet. Chem.* **1985**, *288*, C1−C5.
(38) Simpson, S. J.; Turner, H. W.; Andersen, R. A. *Inorg. Chem.* **1981**, *20*, 2991−2995.
(39) Andersen, R. A.; Zalkin, A.; Templeton, D. H. *Inorg. Chem.* **1981**, *20*, 622−623.
(40) Castro-Rodríguez, I.; Meyer, K. *Chem. Commun.* **2006**, 1353−1368.
(41) Lam, O. P.; Feng, P. L.; Heinemann, F. W.; O'Connor, J. M.; Meyer, K. *J. Am. Chem. Soc.* **2008**, *130*, 2806−2816.
(42) Kozimor, S. A.; Bartlett, B. M.; Rinehart, J. D.; Long, J. R. *J. Am. Chem. Soc.* **2007**, *129*, 10672−10674.
(43) Arnold, P. L.; Pecharman, A.-F.; Hollis, E.; Yahia, A.; Maron, L.; Parsons, S.; Love, J. B. *Nat. Chem.* **2010**, *2*, 1056−1061.
(44) Stewart, J. L.; Andersen, R. A. *Polyhedron* **1998**, *17*, 953−958.
(45) Edwards, P. G.; Andersen, R. A.; Zalkin, A. *J. Am. Chem. Soc.* **1981**, *103*, 7792−7794.
(46) Airoldi, C.; Bradley, D. C.; Chudzynska, H.; Hursthouse, M. B.; Malik, K. M. A.; Raithby, P. R. *Dalton Trans.* **1980**, 2010−2015.
(47) Zalkin, A.; Brennan, J. G.; Andersen, R. A. *Acta Crystallogr., Sect. C* **1988**, *44*, 1553−1554.
(48) Hubert-Pfalzgraf, L. G.; Tsunoda, M.; Le Borgne, G. *J. Chem. Soc., Dalton Trans.* **1988**, 533−535.
(49) Gopinathan, M. S.; Jug, K. *Theo. Chem. Acc.* **1983**, *63*, 497−509.
(50) von Neissen, W. *J. Chem. Phys.* **1972**, *56*, 4290.
(51) Ziegler, T.; Rauk, A. *Inorg. Chem.* **1979**, *18*, 1558.
(52) Ziegler, T.; Rauk, A. *Inorg. Chem.* **1979**, *18*, 1755.
(53) Perrin, L.; Maron, L.; Eisenstein, O. *Faraday Discuss.* **2003**, *124*, 25.
(54) Perrin, L.; Maron, L.; Eisenstein, O.; Lappert, M. F. *New J. Chem.* **2003**, *27*, 121.
(55) Bestmann, H. J.; Stransky, W.; Vostrowsky, O. *Chem. Ber.* **1976**, *109*, 1694−1700.
(56) Bain, G. A.; Berry, J. F. *J. Chem. Educ.* **2008**, *85*, 532.
(57) Berke, C. M.; Streitwieser, A. *J. Organomet. Chem.* **1980**, *197*, 123−134.
(58) *SMART Apex II*, Version 2.1; Bruker AXS Inc.: Madison, WI, 2005.
(59) *SAINT Software User's Guide*, Version 7.34a; Bruker AXS Inc.: Madison, WI, 2005.
(60) Sheldrick, G. M. *SADABS*; University of Göttingen: Göttingen, Germany, 2005.
(61) *SHELXTL PC*, Version 6.12; Bruker AXS Inc.: Madison, WI, 2005.
(62) Perdew, J. P.; Burke, K.; Ernzerhof, M. *Phys. Rev. Lett.* **1996**, *77*, 3865−3868.
(63) Perdew, J. P.; Burke, K.; Ernzerhof, M. *Phys. Rev. Lett.* **1997**, *78*, 1396.
(64) te Velde, G.; Bickelhaupt, F. M.; Baerends, E. J.; Fonseca Guerra, C.; van Gisbergen, S. J. A.; Snijders, J. G.; Ziegler, T. *J. Comput. Chem.* **2001**, *22*, 931−967.
(65) Fonseca Guerra, C.; Snijders, J. G.; te Velde, G.; Baerends, E. J. *Theor. Chem. Acc.* **1998**, *99*, 391−403.